Capillary breakup of a viscous thread surrounded by another viscous fluid

John R. Lister
Institute of Theoretical Geophysics, DAMTP, Cambridge CB3 9EW, England

Howard A. Stone
Division of Engineering & Applied Sciences, Harvard University, Cambridge, Massachusetts 02138

(Received 16 March 1998; accepted 29 July 1998)

Previous long-wavelength analyses of capillary breakup of a viscous fluid thread in a perfectly inviscid environment show that the asymptotic self-similar regime immediately prior to breakup is given by a balance between surface tension, inertia, and extensional viscous stresses in the thread. In contrast, it is shown here that if viscosity in the external fluid, however small, is included then the asymptotic balance is between surface tension and viscous stresses in the two fluids while inertia is negligible. Scaling estimates for this new balance suggest that both axial and radial scales decrease linearly with time to breakup, so that the aspect ratio remains $O(1)$ with time but scales with viscosity ratio like $(\mu_{\rm int}/\mu_{\rm ext})^{1/2}$ for $\mu_{\rm int} \gg \mu_{\rm ext}$, where $\mu_{\rm int}$ and $\mu_{\rm ext}$ are the internal and external viscosities. Numerical solutions to the full Stokes equations for $\mu_{\rm int}=\mu_{\rm ext}$ confirm the scalings with time and give self-similar behavior near pinching. However, the self-similar pinching region is embedded in a logarithmically large axial advection driven by the increasing range of scales intermediate between that of the pinching region and that of the macroscopic drop. The interfacial shape in the intermediate region is conical with angles of about 6° on one side and 78° on the other.
 [S1070-6631(98)01711-5]

I. INTRODUCTION

The capillary instability of a liquid thread is well-known and has many applications. Classical linear theory[1] predicts instability to perturbations with wavelengths greater than the circumference of the thread. Subsequent nonlinear growth of the instability is observed experimentally to lead to disintegration of the thread into droplets, often with the production of many small satellite droplets by secondary instabilities on the fluid filaments left between the primary drops (e.g., Refs. 2–4). A desire to predict the details of satellite-drop formation for industrial processes such as ink-jet printing has motivated many studies of the spatial and temporal development of capillary instabilities on a jet or thread (e.g. Refs. 5–8) by use of experimental, numerical, and weakly nonlinear techniques. A wide-ranging review is given by Eggers.[9]

Recently, however, the focus of attention has switched from the initial development of the instability to the behavior of the flow in the vicinity of the topological singularity when the thread breaks in two. This switch is due partly to the realization that the final stages of pinching affect the subsequent recoil and satellite-drop formation, and partly to a general interest in the formation, structure, and scaling behavior of singularities in nonlinear systems (e.g., Refs. 10–12). Close to the breaking point, the length scales and time scales of motion are orders of magnitude less than those in the far field, which suggests that it is possible to perform a local analysis of the Navier–Stokes equations near the breaking point and seek a self-similar solution for the evolution towards (and after) the singularity.

Since many applications involve liquid threads breaking up in air, it is usually assumed that the external fluid is dynamically passive. Proceeding under this assumption, similarity solutions have been found for the three cases in which the surface-tension-driven dynamics of the internal fluid is controlled by both viscosity and inertia, by viscosity alone, and by inertia alone (finite, zero, and infinite Reynolds numbers).[13–16] Among these solutions, it is asymptotically inconsistent to neglect either inertia or viscosity as the breakup singularity is approached, which is thus predicted to be governed by an inertial-viscous-capillary balance.[13]

The goal of this paper is to reanalyze capillary breakup including the viscous resistance exerted by the external fluid on the motion of the thread. We find that, however small the external viscosity, as the breakup singularity is approached the external viscous shear stresses associated with axial motion of the thread become comparable to the internal viscous stresses associated with extension of the thread. The external viscous ''brake'' slows the flow down and modifies the solution so that the governing asymptotic balance is now between capillary forces and viscous stresses in the two fluids, while the inertial forces are negligible. Since all experiments require an external fluid, it follows that the ''Eggers'' regime[13] is only transitory and will give way to this new viscously dominated regime sufficiently close to the singularity.

The paper is organized as follows. In the next section we use scaling arguments to show why inertia becomes negligible when external viscosity is taken into consideration. Similar arguments are used to predict power-law scalings for the axial, radial, and velocity scales as functions of the time remaining to breakup. Sections III and IV describe numerical calculations of capillary breakup for the case in which the internal and external fluids are in Stokes flow and are of

equal viscosity. The calculations confirm the simple scalings of Sec. II and give self-similar evolution, but also show that the axial velocity in the pinching region increases logarithmically as the time to the singularity decreases. This result is surprising since the locally driven flow is estimated as $O(1)$, and this stands in contrast to the previous analyses without external viscosity in which the velocity can be estimated by local scalings. The explanation for the increase of the axial velocity in terms of flow driven by conical intermediate regions on either side of the pinch is described in Sec. V and a summary of our findings is given in Sec. VI. In the Appendix we outline a simple one-dimensional long-wavelength model of breakup for the case when the external fluid is much less viscous than the internal. Such localized long-wavelength models have been valuable in previous studies, but the simple model outlined here seems to lack the proper coupling between local and nonlocal effects to reproduce the dynamics seen in Secs. III and IV.

II. SCALING ARGUMENTS

Consider the dynamics of an axisymmetric fluid thread of radius $h(z,t)$, viscosity μ, density ρ, and surface tension γ in a surrounding fluid of viscosity μ_{ext} and density ρ_{ext}. Neglecting the influence of the external fluid ($\mu_{\text{ext}}=0$), Eggers[13] argued that the flow in the neighborhood of and immediately prior to breakup is described by a long-wavelength approximation to the Navier–Stokes equations in which the axial velocity $v(z,t)$ is uniform across the thread and the dynamics is given by a balance between the axial gradient of the capillary pressure, the axial acceleration, and the internal viscous resistance to extension of the thread. If we combine the dynamic balances $\gamma\partial(h^{-1})/\partial z \sim \rho\partial v/\partial t \sim \mu\partial^2 v/\partial z^2$ with the kinematic estimate $v\sim z/\tau$, where τ is the time remaining to a breakup at $z=0$, then we obtain the scalings

$$z\sim l_\mu\left(\frac{\tau}{t_\mu}\right)^{1/2}, \quad h\sim l_\mu\left(\frac{\tau}{t_\mu}\right), \quad v\sim\frac{\gamma}{\mu}\left(\frac{\tau}{t_\mu}\right)^{-1/2}, \tag{1}$$

which are the basis of the similarity solutions found in Refs. 13 and 15. Here $l_\mu=\mu^2/(\gamma\rho)$ and $t_\mu=\mu^3/(\gamma^2\rho)=\mu l_\mu/\gamma$ are the natural fluid-dependent length scale and time scale on which the similarity solutions are valid. In this regime the Reynolds number $\mathrm{Re}=\rho v z/\mu$ is $O(1)$.

We note that for water $l_\mu\sim 10^{-8}$ m and $t_\mu\sim 10^{-10}$ s, whereas for syrup $l_\mu\sim 10$ m and $t_\mu\sim 10^{3}$ s, which suggests that breakup on laboratory (millimeter) scales will have a significant inertially dominated or viscously dominated transient. Indeed, if the length scale of the initial conditions is l_0 then the initial dynamical response can be characterized by the magnitude of a Reynolds number $\mathrm{Re}_0=\rho\gamma l_0/\mu^2=l_0/l_\mu$ (the inverse of the Ohnesorge number). A viscous-capillary balance $\gamma\partial(h^{-1})/\partial z\sim\mu\partial^2 v/\partial z^2$ ($\mathrm{Re}_0\ll 1$), together with $v\sim z/\tau$, gives

$$z\sim l_0\left(\frac{\tau}{t_0}\right)^{\beta}, \quad h\sim l_0\left(\frac{\tau}{t_0}\right), \quad v\sim\frac{\gamma}{\mu}\left(\frac{\tau}{t_0}\right)^{\beta-1}, \tag{2}$$

where the choice of l_0 as length scale is arbitrary, $t_0=\mu l_0/\gamma$, and the exponent β is determined as a nonlinear eigenvalue of the resulting similarity equations.[14,15] Since $\mathrm{Re}\sim\mathrm{Re}_0(\tau/t_0)^{2\beta-1}$ and the maximum value of β is 0.175, the neglect of inertia is invalid as $\tau\to 0$. An inertial-capillary balance $\gamma\partial(h^{-1})/\partial z\sim\rho\partial v/\partial t$ ($\mathrm{Re}_0\gg 1$) with $v\sim z/\tau$ also appears at first sight to leave an exponent β to be determined from the similarity equations.[17] However, numerical solutions of breakup in potential flow[16] show that the Laplacian operator imposes $h\sim z$, which gives similarity solutions with the scalings

$$h\sim z\sim\left(\frac{\gamma\tau^2}{\rho}\right)^{1/3}, \quad v\sim\left(\frac{\gamma}{\rho\tau}\right)^{1/3}. \tag{3}$$

Since $h\sim z$, the far-field shape is predicted to be conical, in agreement with numerical solutions.[16] Since $\mathrm{Re}\sim(\rho\gamma^2\tau)^{1/3}/\mu$, the neglect of viscosity is invalid as $\tau\to 0$.

Considerations thus far suggest that (1) is the final scaling prior to breakup. However, axial motion of the breaking thread drives a flow in the surrounding fluid, the vorticity of which can diffuse a distance of order $(\mu_{\text{ext}}\tau/\rho_{\text{ext}})^{1/2}$ from the thread, which, as $h\sim\tau$ from (1), corresponds to many thread radii as $\tau\to 0$. Hence the external fluid responds as a viscously dominated flow outside an axially sliding cylinder and exerts a shear stress of order $\mu_{\text{ext}}\partial v/\partial r$ on the thread or, equivalently, makes a contribution of order $\mu_{\text{ext}}\partial^2 v/\partial r^2$ to the axial momentum balance. Using $r\sim h$ and (1), this contribution is found to be proportional to $\tau^{-5/2}$ as $\tau\to 0$, whereas the capillary, inertial, and internal viscous terms are proportional to $\tau^{-3/2}$. It follows that, unless $\mu_{\text{ext}}\equiv 0$, the neglect of the external fluid eventually becomes invalid and the flow makes a transition to a new dynamical balance (assuming, of course, that molecular dimensions are not reached first).

When the external viscous drag is reintroduced, the scalings for the new balance can most simply be obtained from $\gamma\partial(h^{-1})/\partial z\sim\mu\partial^2 v/\partial z^2\sim\mu_{\text{ext}}\partial^2 v/\partial r^2$, together with $v\sim z/\tau$, which gives

$$z\sim\frac{\gamma\tau}{m^{1/2}\mu}, \quad h\sim\frac{\gamma\tau}{\mu}, \quad v\sim\frac{\gamma}{m^{1/2}\mu}, \tag{4}$$

where $m=\mu_{\text{ext}}/\mu$. Since $z\sim h$ as $\tau\to 0$, a similarity solution for breakup based on these scalings would be expected to have the properties that the quasisteady regions on either side of localized rapid pinching would be asymptotically conical, $h\sim m^{1/2}z$, and that characteristic velocities in the pinching region, such as the maximum velocity, would be constant.

A number of further points should be noted. First, since we have been assuming implicitly in our scalings that the axial length scale and velocity scale close to breakup are either comparable to or much greater than the radial scales, (4) is only appropriate if μ is comparable to or much greater than μ_{ext}; the breakup of an inviscid bubble in a viscous environment may require separate analysis. Second, since z and h have the same time dependence, use of a long-wavelength (slender-body) approximation in the Appendix relies on $m\ll 1$ or $\mu_{\text{ext}}\ll\mu$ rather than on asymptotic behavior in time. Third, the Reynolds number based on (4), $\mathrm{Re}\sim\tau/(t_\mu m^{1/2})$, is proportional to τ confirming that the inertial terms are asymptotically small.

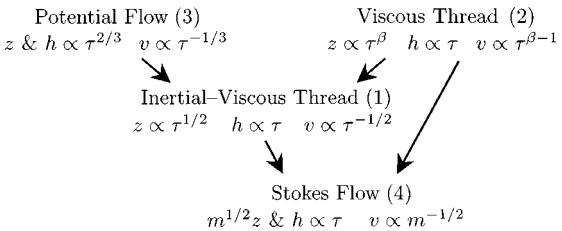

FIG. 1. The scalings and temporal transitions between the various dynamical regimes for capillary breakup; $m=\mu_{\rm ext}/\mu$. The transition from the inertial-viscous thread to the two-fluid Stokes flow occurs when $z \sim m^{1/2}\mu^2/(\gamma\rho)$, $h \sim m\mu^2/(\gamma\rho)$, and $\tau \sim m\mu^3/(\gamma^2\rho)$.

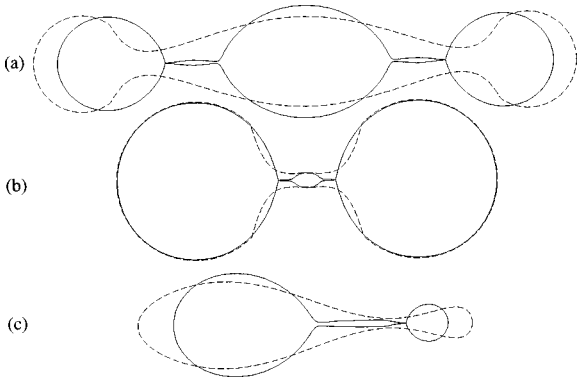

FIG. 2. Initial (dashed) and final (solid) shapes from three simulations (a)–(c).

It is possible for capillary breakup to pass through a number of these different dynamical regimes as the scales of the pinching region and velocity evolve. The transition from (1) to (4) occurs when $z \sim m^{1/2} l_\mu$, $h \sim m l_\mu$, and $\tau \sim m t_\mu$; for some common pairs of fluids, such as water pinching in air, this transition is on molecular scales and beyond the applicability of continuum mechanics. Depending on the relative sizes of the initial Reynolds number $\mathrm{Re}_0=\rho\gamma l_0/\mu^2$ and the viscosity ratio m, it is also possible for a flow to make a transition directly from (2) to (4) without passing through the intermediate scaling (1). The possible transitions are summarized in Fig. 1. The transition scales between regimes can be determined by the crossovers between Eqs. (1) and (4) and used to interpret the dynamical regime corresponding to particular experimental observations.

III. STOKES FLOW SIMULATIONS

The scalings of the previous section show that the asymptotic dynamical balance for capillary breakup is viscously dominated both inside and outside the pinching thread. Motivated by this, we present calculations for the capillary-driven breakup of a fluid drop in which both the drop and its environment are in Stokes flow. Similar calculations are underway by Loewenberg and co-workers.[18]

Let the drop surface $S(t)$ have outward normal $\mathbf{n}$ and curvature κ so that the flow is driven by a capillary jump in stress $\gamma\kappa\mathbf{n}$ across S. We make all velocities dimensionless with respect to the scale γ/μ and choose an arbitrary length scale (e.g., the initial radius of the drop) to scale all lengths. The dimensionless internal viscosity is then 1 and the external viscosity m. The velocity for points $\mathbf{x} \in S(t)$ has the exact boundary-integral representation[19]

$$\frac{1}{2}(1+m)\mathbf{u}(\mathbf{x}_s)+(m-1)\int_{\mathbf{y}\in S(t)} \mathbf{n}\cdot\mathbf{K}\cdot\mathbf{u}\, dS_{\mathbf{y}} = -\int_{\mathbf{y}\in S(t)} \kappa\mathbf{n}\cdot\mathbf{J}\, dS_{\mathbf{y}}, \tag{5}$$

where

$$\mathbf{J}(\mathbf{r})=\frac{1}{8\pi}\left[\frac{\mathbf{I}}{r}+\frac{\mathbf{rr}}{r^3}\right], \quad \mathbf{K}(\mathbf{r})=-\frac{3}{4\pi}\frac{\mathbf{rrr}}{r^5}, \quad \mathbf{r}=\mathbf{x}-\mathbf{y}, \tag{6}$$

and $dS_{\mathbf{y}}$ is the scalar element of area on $S(t)$ at $\mathbf{y}$.

For simplicity, we restrict our attention to axisymmetric configurations so that the azimuthal integral can be performed analytically, and to equal viscosities ($m=1$) so that $\mathbf{u}$ is obtained directly as an integral of the curvature rather than as the solution of an integral equation. Equation (5) can then readily be solved using a boundary-element method, the details of which are very similar to those described in Ref. 20. The evolution of an initial ''dog-bone'' shape is followed by calculating the interfacial velocity from a discretized version of (5), moving marker points distributed along the interface with the local normal component of velocity, and then repeating the procedure. Marker points were added and redistributed along the interface in such a way as to maintain a smoothly varying spacing proportional to the local curvature in order to resolve the details of flow near the highly curved pinching region. In the calculations reported here, the initial shapes were represented by about 200 points and the final shapes, in which the minimum radius had decreased to roughly 10^{-10}, were represented by about 4000 points, most of them concentrated near the pinching region. Each time step was chosen to be about 0.5% of the current minimum radius divided by the radial velocity at the minimum, so that each decade of reduction in the minimum radius required about 500 time steps. Test calculations with double the density of marker points and with half the time step yielded the same results as those given below.

IV. RESULTS

The initial and final shapes from three simulations are shown in Fig. 2 and a number of aspects of the evolution of one simulation in Fig. 3. In each simulation, regions initially with a single minimum radius develop two pinching minima, which suggests a strong propensity for satellite-drop formation in Stokes flow, as in other dynamical regimes. Pinching always occurs asymmetrically, which is like calculations with internal inertia but no external drag[13,15,16] and unlike calculations without either internal inertia or external drag.[14] To a very good approximation, the shape on either side of the pinching region is conical [Fig. 3(B)] and the minimum radius $h_{\rm min}$ decreases linearly with time [Fig. 3(C)], which is in agreement with the scaling predictions $h \sim z \sim \tau$ given earlier. The axial strain is concentrated in the pinching region

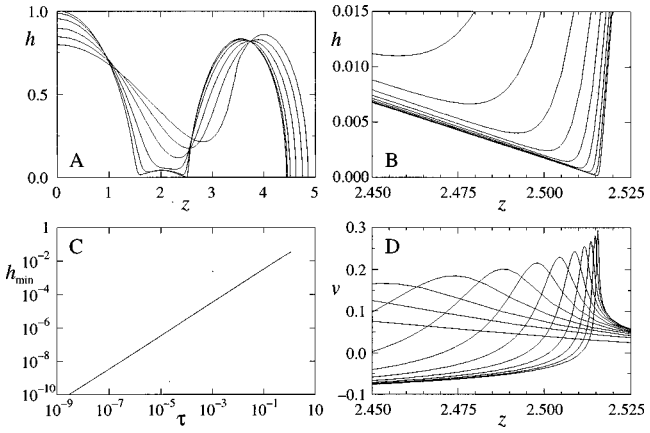

FIG. 3. Evolution with time of simulation (a). (A) The early global evolution of the shape; (B) enlargement showing the local double-cone structure; (C) the minimum radius versus time remaining to breakup; (D) the local axial velocity.

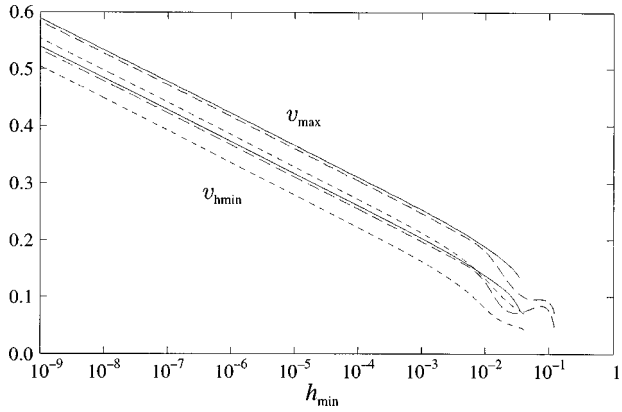

FIG. 5. A plot of $v_{h\min}$ and $v_{\max}$ against $h_{\min}$ shows a linear increase with $\ln h_{\min}$ for each simulation shown in Fig. 2 (simulation a: solid; b: long-dashed; c: short-dashed).

[Fig. 3(D)] and, whereas the prediction $v \sim 1$ suggests the velocity scale should be constant, the maximum axial velocity increases steadily.

In order to get a better understanding of the behavior as the point of breakup is approached, we define rescaled variables

$$H = h/h_{\min} \quad \text{and} \quad \zeta = (z - z_{h\min})/h_{\min}, \tag{7}$$

where $z_{h\min}$ is the axial location of the minimum radius $h_{\min}$. Rescaling all lengths with $h_{\min}$ in this way allows a better test of self-similarity than rescaling with τ since the latter requires estimation of the origin of τ. Figure 4 shows profiles of various rescaled variables for shapes spanning the six decades $10^{-3} > h_{\min} > 10^{-9}$ from the three simulations. There is very good collapse of the profiles of $H(\zeta)$ [Fig. 4(A)], the axial curvature $H''(\zeta)/[1+H'^2]^{3/2}$ [Fig. 4(B)], and the axial strain rate $v'(\zeta)$ [Fig. 4(C)], where primes denote $\partial/\partial\zeta$.

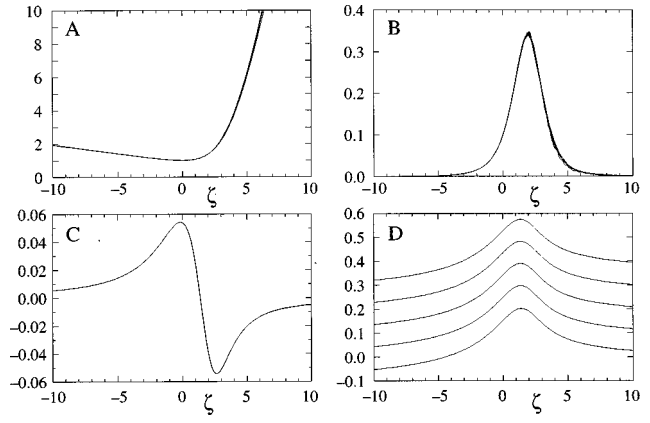

FIG. 4. Local shapes and velocity fields rescaled with $h_{\min}$ according to $H = h/h_{\min}$ and $\zeta = (z - z_{h\min}/h_{\min}$ over the approximate range $10^{-3} > h_{\min} > 10^{-9}$. Graphs (A) and (B) show three profiles from each of the three simulations; graphs (C) and (D) show five profiles from simulation (c). The collapse of the data is very good, suggesting self-similarity, except for v. (A) $H(\zeta)$; (B) $H''/[1+H'^2]^{3/2}$; (C) v'; and (D) v.

These results suggest that the evolution is indeed self-similar. The axial velocity v [Fig. 4(D)], however, increases steadily as $h_{\min}$ decreases.

A plot of a characteristic axial velocity (Fig. 5), such as the value $v_{h\min}$ at the minimum radius $h_{\min}(\zeta=0)$ or the value of the maximum $v_{\max}$ near $\zeta=1.4$, shows that the increase in velocity is very well described by the log-linear form $v = -0.0243 \ln h_{\min} + \text{const}$, where the constant depends on which point of the profile is chosen and which simulation is considered. We argue below that the logarithmically increasing component of the flow is induced by that part of the interface in $1 \ll |\zeta| \ll h_{\min}^{-1}$ (or $h_{\min} \ll |z - z_{h\min}| \ll 1$) and show that the coefficient 0.0243 can be predicted from a double-cone approximation for the shapes on either side of the pinching region. For the moment, we note that deformation of the interface can only be produced by strain and not by a uniform velocity. Thus the primary effect of the logarithmically increasing velocity component in the pinching region is simply to advect it without deformation, while the local deformation is achieved by the self-similar strain field [Fig. 4(C)].

Further tests of self-similarity in the pinching region were made by considering the variation (Fig. 6) with $h_{\min}(t)$ of variables such as $dh_{\min}/dt$, the maximum value of H' on the shallow side (which occurs near $\zeta=-8$), and the axial curvature at the minimum $H''(0)$. All were found to be asymptotically constant as $h_{\min}(t) \to 0$, thus confirming self-similarity. The convergence in these tests was found to be significantly improved by subtracting the maximum axial velocity from the velocity at every grid-point, updating the interface with the normal component of the residual, and then translating every grid-point by a distance corresponding to the subtracted maximum velocity. The effect of this procedure is to use a suitably translating reference frame in which numerical errors associated with the large axial advection are eliminated in the pinching region and shifted to the distant parts of the drop.

Finally, we observe that the asymptotic shape of the drop in $1 \ll |\zeta| \ll h_{\min}^{-1}$ is conical as predicted by the scaling theory, and that the asymptotic slopes are found numerically to be 0.103 and 4.8, corresponding to angles 5.9° and 78.2°. It is

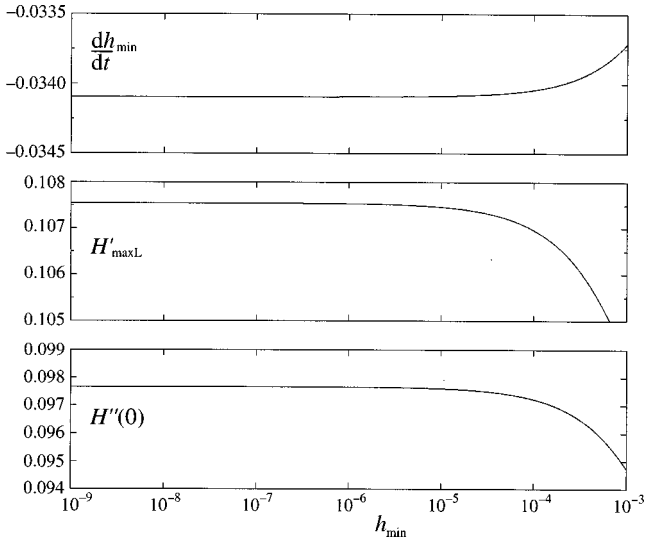

FIG. 6. Convergence towards self-similarity as $h_{\min}\to 0$ is revealed by: $dh_{\min}/dt$, the maximum H' on the shallow side, and the axial curvature at the minimum $H''(0)$.

interesting to contrast these angles with the cone angles formed by capillary pinching of an inviscid drop, which were found numerically to be 18.1° and 112.8°.[16]

V. DISCUSSION OF AXIAL VELOCITY

The numerical results presented above show that the near-pinching solution for Stokes flow is self-similar with scalings $h\sim z\sim\tau$. A significant difference from the self-similar behavior found in other dynamical regimes is that there is a large locally uniform axial velocity, increasing linearly with $\ln h_{\min}$, superposed on and dominating the local strain field in the pinching region. We have seen that this does not prevent self-similarity in an appropriately rapidly translating reference frame. It remains, however, to interpret the large axial velocity.

The assumption of a local similarity solution is based on the separation between the length scale of the pinching region $l_\tau=\gamma\tau/\mu$ (note $h_{\min}\sim l_\tau$) and the macroscopic length scale l_0 as $\tau\to 0$. The flow can be divided into the curved neck of the pinching region $z=O(l_\tau)$, an intermediate region $l_\tau\ll|z|\ll l_0$ in which the interface is asymptotically conical, and the macroscopic far field $z=O(l_0)$. (For simplicity, we choose axes with $z_{h\min}=0$ here.) The velocity field in the pinching region is an integral of the interfacial curvature over contributions from all three regions as expressed in (5), and it is instructive to consider the role of the three contributions.

The contribution from curvature in the far field is a velocity with an $O(l_0)$ scale of variation, which looks like a uniform and constant velocity of translation on the short length scale and time scale of the pinching region and thus plays no role in the pinching dynamics. This additive constant probably accounts for the small, consistent difference between the axial velocities in different simulations which have a different macroscopic shape (Fig. 5). The contribution to the velocity from the curvature in the pinching region itself, where capillary stresses are $O(\gamma/l_\tau)$ on a length scale l_τ, is $O(\gamma/\mu)$ with a length scale of variation $O(l_\tau)$. A purely local solution would have pinching dynamics governed solely by interfacial motion in this region. However, the contribution from the conical intermediate region is driven by a capillary stress proportional to γ/z. Thus either direct estimation or calculation of separable solutions for Stokes flow in a cone shows that the shear rate is proportional to $\gamma/(\mu z)$ and hence that this contribution to the velocity is $O[(\gamma/\mu)\ln(l_0/l_\tau)]$.

A simple calculation confirms that the contribution of the intermediate region is responsible for the linear increase (Fig. 5) of the axial velocity in the pinching region with $\ln h_{\min}$. A perfect cone of half angle α has normal $\mathbf{n}=(-\cos\alpha,\ \sin\alpha)$, curvature $\kappa=1/(r\tan\alpha)$, and surface element $dS=2\pi r\sin\alpha\, dr$, where r is the radial distance from the apex. If the cone has extent $0<r<R$ then (5) with $m=1$ gives an axial velocity

$$v(0,z)=\frac{\gamma}{4\mu}\sin\alpha\cos\alpha\int_0^R\frac{(r^2-3\cos\alpha rz+2z^2)dr}{(r^2-2\cos\alpha rz+z^2)^{3/2}}. \tag{8}$$

As $z/R\to 0$, this integral (which can be done analytically if desired) is dominated by an $O[\ln(R/z)]$ contribution from $z\ll r\ll R$. The dominant contribution from a perfect double cone with slopes $t_L=\tan\alpha_L$ and $t_R=\tan\alpha_R$ is found to be

$$v(z,0)\sim\frac{\gamma}{4\mu}\left(\frac{t_R}{t_R^2+1}-\frac{t_L}{t_L^2+1}\right)\ln\left(\frac{R}{|z|}\right)+\text{const}\quad\text{as}\quad z/R\to 0. \tag{9}$$

Thus the conical regions pull in opposite directions with the side with the angle closest to 45° ($\tan\alpha=1$) wining the tug-of-war. Taking $t_L=0.103$ and $t_R=4.8$ from the numerical solutions, we find $v\sim 0.024\ln(R/|z|)+\text{const}$, which is in good agreement with the observed $v\sim -0.0243\ln(h_{\min})+\text{const}$ if we make the obvious identification $R=l_0$ and $z=h_{\min}\propto l_\tau$. The effects of the flow induced by the intermediate region are confined to simple advection of the pinching region since, as with the flow driven by the far field, the length scale of the strain driven by the intermediate region is much greater than l_τ.

VI. CONCLUSIONS

The most important conclusion is that including the effects of viscosity in the outer fluid modifies the asymptotic structure of capillary breakup near the singularity: external shear stresses become comparable to the internal extensional stresses and the capillary driving, and inertia becomes negligible. The aspect ratio of the pinching region is roughly constant with time, rather than asymptotically small, and hence this regime is best described by the Stokes equations in both fluids and the full expression for the curvature, rather than by a long-wavelength approximation. In the limit $\mu\gg\mu_{\text{ext}}$ the aspect ratio is predicted by scaling arguments to be $O(\mu_{\text{ext}}/\mu)^{1/2}$, but still constant.

It should be noted that, while two-fluid Stokes flow is the theoretical asymptotic regime close to the singularity, some pairs of common experimental fluids, such as water

pinching in air, will reach molecular scales before this regime. The transitions from other dynamical regimes are summarized in Fig. 1 and the transition scales readily derived by comparison of (1)–(4).

Numerical solutions of the Stokes equations with $\mu = \mu_{\text{ext}}$ show that: the minimum radius and the axial scale of the pinching region are asymptotically proportional to the time remaining to breakup; the shape on either side of the pinching region is asymptotically conical with one side steep ($\approx 78°$) and the other shallow ($\approx 6°$); the shape and strain rate in the pinching region are self-similar when scaled by the time-dependent minimum radius. These results are in agreement with simple scaling theory. The similarity solution is embedded in a logarithmically large flow induced by the conical regions intermediate between the scale of the minimum radius and the macroscopic scale of the drop.

We believe similar results to the above will hold in the case of unequal viscosities, though we have not yet studied this owing to the cost of solving (5) with $m \neq 1$. We investigated a simple long-wavelength model for the limit $\mu \gg \mu_{\text{ext}}$ in which the external fluid is represented by a local linear drag term (Appendix), but concluded that the approximations made did not capture the essential dynamics. It is probably best to deal with the case of unequal viscosities by directly solving the integral equation for the similarity shapes in the pinching region, after taking due account of the logarithmically infinite contribution to the velocity from the far field.

ACKNOWLEDGMENTS

The authors thank M. P. Brenner for help, advice, and encouragement throughout this project. Conversations with J. Eggers are also gratefully acknowledged.

APPENDIX: A SIMPLE SLENDER-BODY ANALYSIS

The scaling in (4) shows that in the limit $\mu_{\text{ext}} \ll \mu (m \ll 1)$ the axial length scale must be much greater than the radial length scale if the internal and external viscous stresses are to be comparable. This observation suggests that a long-wavelength approximation might be appropriate as $m \to 0$, which would have the advantage not only of simplifying the problem to a one-dimensional model but also establishing a connection to one-dimensional studies of pinching in the absence of external viscosity (e.g., Refs. 13–15).

In the long-wavelength limit, the internal velocity v is nearly uniform across the thread's cross section and the internal viscous stress is dominated by axial extension; the external viscous stresses are analogous to those that arise when a cylinder is dragged along its length in a viscous fluid (cf. the ''sliding-rod'' regime of Ref. 23). These ideas suggest a simple one-dimensional model

$$(h^2)_t + (h^2 v)_z = 0, \tag{A1}$$

$$\frac{3\mu}{h^2}(h^2 v_z)_z - \beta \mu_{\text{ext}} \frac{v}{h^2} = \gamma \left(\frac{1}{h} - h_{zz} \right)_z, \tag{A2}$$

where the external drag term reflects a local velocity difference v between the thread and ambient stationary fluid over a radial length scale h and β is a dimensionless coefficient. In the context of slender-body theory[21,22] this drag term can be derived rigorously by asymptotic expansion of (5) as $m \to 0$ (e.g., Ref. 23) and β identified as $2/|\ln \epsilon|$, where ϵ is the ratio of the radial and axial dimensions of a translating finite slender body. In the present context, we might hope that setting ϵ equal to the expected ratio of radial and axial scales would lead to a useful heuristic model.

Equations (A1) and (A2) can be made dimensionless by rescaling axial distances by an arbitrary length scale l, radial distances by ϵl, and axial velocities by $\gamma/\epsilon\mu$, where $\epsilon^2 |\ln \epsilon| = m \ll 1$. Equation (A1) is unaltered, while (A2) becomes

$$3(h^2 v_z)_z = 2v + h^2 \left(\frac{1}{h} - \epsilon^2 h_{zz} \right)_z. \tag{A3}$$

Though the h_{zz} term is asymptotically smaller in ϵ than the other terms, it is sometimes retained to stabilize the slender thread against secondary Rayleigh instabilities with wavelengths much less than the primary pinching length scale.[4,15]

The slender-body partial differential equations (A1) and (A3) are very similar to others which give local similarity solutions by substitution of the obvious scalings and solution of the resultant ordinary differential equations (ODEs).[13–15] Following the standard protocol, we would substitute $h(z,t) = \tau H(\eta)$, $v(z,t) = V(\eta)$, and $\eta = z/\tau$ into (A1) and (A3) to obtain

$$\frac{H'}{H} = \frac{2 - V'}{2\eta + 2V}, \quad V = 2H' + 3(H^2 V')', \tag{A4}$$

where the h_{zz} term is assumed here to be asymptotically negligible. Analysis of these ODEs follows very closely that in Ref. 15, but no solutions satisfying both the ''forward'' boundary condition at $\eta = +\infty$ or the ''backward'' boundary condition at $\eta = -\infty$ were found. The lack of a simple similarity solution is in agreement with a lack of self-similarity observed in numerical simulations of the full time-dependent problem (A1) and (A3). These simulations do show asymmetric pinching, roughly linear scaling of dimensions with τ, and roughly conical regions on either side of the pinch, as would be expected from naive scaling. However, they differ from our simulations of the Stokes equations in that the axial scale does not collapse with h_{min} (cf. Fig. 4) and the increase in the axial velocity is not linear with $\ln h_{\text{min}}$ (cf. Fig. 5); the slopes of the near-cones also depend strongly on the value of ϵ.

We believe the reason for these differences is that the local linear drag term does not properly capture the nonlocal influence of the intermediate region, which we have shown generates the large axial velocity in the pinching region. In the Stokes equations the intermediate region communicates with the pinching region by driving flows in both the ambient and pinching fluids (and hence advection), whereas in (A3) communication is by tension (and hence deformation) in the thread and the ambient fluid is assumed implicitly to be at rest; exact double-cone solutions to (A3) have an algebraic rather than logarithmic dependence of v on z. We note that this difference cannot simply be rectified by making the

drag term proportional to $v-v_\infty$ with a constant v_∞. It is possible that a nonlocal term, such as a one-dimensional Hilbert integral, might rectify the problem.

[1]Lord Rayleigh, ''On the stability of a cylinder of viscous fluid under a capillary force,'' Philos. Mag. **34**, 145 (1892).
[2]T. A. Kowalewski, ''On the separation of droplets from a liquid jet,'' Fluid Dyn. Res. **17**, 121 (1996).
[3]D. M. Henderson, W. G. Pritchard, and L. B. Smolka, ''On the pinch-off of a pendant drop of viscous fluid,'' Phys. Fluids **9**, 3188 (1997).
[4]M. P. Brenner, X. D. Shi, and S. R. Nagel, ''Iterated instabilities during droplet fission,'' Phys. Rev. Lett. **73**, 3391 (1994).
[5]H. C. Lee, ''Drop formation in a liquid jet,'' IBM J. Res. Dev. **18**, 364 (1974).
[6]D. B. Bogy, ''Drop formation in a circular liquid jet,'' Annu. Rev. Fluid Mech. **11**, 207 (1979).
[7]K. C. Chaudhary and L. G. Redekopp, ''The nonlinear capillary instability of a liquid jet. Part 1. Theory,'' J. Fluid Mech. **96**, 257 (1980).
[8]M. Tjahjadi, H. A. Stone, and J. M. Ottino, ''Satellite and subsatellite formation in capillary breakup,'' J. Fluid Mech. **243**, 297 (1992).
[9]J. Eggers, ''Nonlinear dynamics and breakup of free-surface flows,'' Rev. Mod. Phys. **3**, 865 (1997).
[10]R. E. Caflisch and G. C. Papanicolaou, *Singularities in Fluids, Plasmas, and Optics*, volume C404 of NATO ASI Series (Kluwer Academic, Dordrecht, 1993).
[11]R. E. Goldstein, A. I. Pesci, and M. J. Shelley, ''Topology transitions and singularities in viscous flows,'' Phys. Rev. Lett. **70**, 3043 (1993).
[12]M. C. Pugh and M. J. Shelley, ''Singularity formation in thin jets with surface tension,'' Commun. Pure Appl. Math. **51**, 733 (1998).
[13]J. Eggers, ''Universal pinching of 3D axisymmetric free-surface flow,'' Phys. Rev. Lett. **71**, 3458 (1993).
[14]D. Papageorgiou, ''On the breakup of viscous liquid threads,'' Phys. Fluids **7**, 1529 (1995).
[15]M. P. Brenner, J. R. Lister, and H. A. Stone, ''Pinching threads, singularities and the number 0.0304...,'' Phys. Fluids **8**, 2827 (1996).
[16]R. F. Day, E. J. Hinch, and J. R. Lister, ''Self-similar capillary pinchoff of an inviscid fluid,'' Phys. Rev. Lett. **80**, 704 (1998).
[17]L. Ting and J. B. Keller, ''Slender jets and thin sheets with surface tension,'' SIAM (Soc. Ind. Appl. Math.) J. Appl. Math. **50**, 153 (1990).
[18]J. Bawzdziewicz, V. Christini, and M. Loewenberg, ''Analysis of drop breakup in creeping flows,'' Bull. Am. Phys. Soc. **42**, 2125 (1997).
[19]J. M. Rallison and A. Acrivos, ''A numerical study of the deformation and burst of a viscous drop in an extensional flow,'' J. Fluid Mech. **89**, 191 (1978).
[20]H. A. Stone and L. G. Leal, ''The effect of surfactants on drop deformation and breakup,'' J. Fluid Mech. **220**, 161 (1990).
[21]G. K. Batchelor, ''Slender-body theory for particles of arbitrary cross-section,'' J. Fluid Mech. **44**, 419 (1970).
[22]R. G. Cox, ''The motion of long slender bodies in a viscous fluid. Part 1 General theory,'' J. Fluid Mech. **44**, 791 (1970).
[23]J. R. Lister and H. A. Stone, ''Time-dependent viscous deformation of a drop in a rapidly rotating denser fluid,'' J. Fluid Mech. **317**, 275 (1996).